Antibody-Catalyzed Hydrolysis of Enol Ethers. 2. Structure of the Antibody-Transition State Complex and Origin of the Enantioselectivity

Guiti K. Jahangiri and Jean-Louis Reymond*

Contribution from the Department of Molecular Biology, The Scripps Research Institute, 10666 North Torrey Pines Road, La Jolla, California 92037

Received June 15, 1994[⊗]

Abstract: The hydrolysis of alkyl enol ethers to their corresponding carbonyl compounds proceeds by acid-catalyzed, rate-determining protonation on the β-carbon to form an oxocarbonium ion intermediate (Kresge, A. J.; Chang, Y. *J. Chem. Soc. B* **1967**, 53). Antibody 14D9 (anti-**1**) catalyzes the hydrolysis of enol ethers **4** and **5** with very high enantioselectivity of protonation (Reymond, J.-L.; Janda, K. D.; Lerner, R. A. *J. Am. Chem. Soc.* **1992**, *114*, 2257). Catalysis involves participation of an antibody side chain as a general acid, as well as pyramidalization of the enol ether's β-carbon by hydrophobic contacts between its substituents and the antibody (Reymond, J.-L.; Jahangiri, G. K.; Stoudt, C.; Lerner, R. A. *J. Am. Chem. Soc.* **1993**, *115*, 3909). The present study addresses the question of the origin of the enantioselectivity of this catalyst. First, enantioselectivity and substrate tolerance, which are most remarkable in antibody 14D9, are shown to be recurrent features for anti-**1** or anti-**2** antibodies. Four antibodies were studied, and all enantioselectively deliver a proton on the *re* face of enol ethers to produce (*S*)-configured carbonyl products, while stereoselectively binding to analogs of the (*S,S*)-hapten **1**. The orientation of the enol ether at the transition state relative to the hapten is then established by comparing the effect of alkyl substitutions at the β-carbon on antibody catalysis with the effect of equivalent substitutions on antibody binding to hapten analogs. For antibody 14D9 (anti-**1**), the results show that the alkyl substituent of the enol ether's β-carbon binds to the *N*-methyl site of the hapten at the transition state. Substitution of ethyl for methyl at that position results in a 20-fold drop in transition state binding and a 3-7-fold drop in affinity for inhibitors. The orientation is such that the cyclic substrates do not fit in the site complementary to the piperidine ring of the hapten at the transition state. The antibody-catalyzed hydrolysis of the cyclopentanone enol ether **6**, which produces exclusively (*S*)-**7**, is 40 times more efficient than for the cyclohexanone enol ether **10**. By contrast, no binding selectivity is found for the individual enantiomers of the corresponding ketone products **7** and **18**, which are neutral transition state analogs for *re*- or *si*-selective protonation of **6** or **10**. The enantioselectivity of 14D9 appears only for the transition state, which suggests that it contains a dynamic component, probably the strict geometrical constraint that the enol ether be aligned with the antibody residue acting as a general acid catalyst during proton transfer. The enantioselectivity of antibody 14D9 thus results from an unexpected combination of binding and catalysis. This study establishes the relationship between hapten and transition states in unprecedented details. The observation that the discriminating power of an antibody for enantiomeric transition states can far exceed simple binding discrimination for ground state molecules suggests a promising future for catalytic antibodies as enantioselective catalysts.

Introduction

The structure and function of natural enzymes are extremely complex. Nevertheless, catalysis by enzymes can be reduced to the simple concept of selective binding to the transition state.[1] Antibodies, which can be instructed to bind ground state molecules during immunization, can be turned into enzyme-like catalysts by directing them against stable transition state analogs of chemical reactions. This idea[2] was first demonstrated in 1986 by Lerner and Schultz using monoclonal antibodies, and has opened a new era in catalyst design.[3] The method has been so successful that the number of new catalytic antibodies generated has grown faster than their detailed understanding. This reflects the fact that it is extremely difficult to estimate how far a catalytic antibody actually operates according to the "planned" reaction pathway encoded in the structure of the transition state analog used as hapten.

We recently reported that antibodies raised against haptens **1**-**3**[4] catalyze the hydrolysis of enol ethers **4** and **5**[5] (Scheme 1). The reaction involves rate-determining proton transfer to the β-carbon atom of the enol ether, forming a reactive oxocarbonium ion intermediate (**I**), which then reacts with a molecule of water to a hemiacetal and ultimately the carbonyl product.[6] For one of them (14D9, anti-**1**), the reaction was shown to produce enantiomerically pure carbonyl compounds. The process could readily be scaled up to produce gram quantities of optically active ketone (−)-(*S*)-**7**, demonstrating the potential of this catalytic antibody as a catalyst for organic synthesis.[7] 14D9 hydrolyzes a relatively broad variety of enol ethers possessing the aromatic nucleus (Ar), which is necessary as the recognition element. The best substrates have (*Z*)

[⊗] Abstract published in *Advance ACS Abstracts*, November 15, 1994.

(1) Pauling, L. *Am. Sci.* **1988**, *36*, 51.

(2) Jencks, W. *Catalysis in Chemistry and Enzymology;* McGraw-Hill: New York, 1969.

(3) Reviews: (a) Lerner, R. A.; Benkovic, P. G.; Schultz, P. G. *Science* **1991**, *252*, 659-667. (b) Schultz, P. G.; Lerner, R. A. *Acc. Chem. Res.* **1993**, *26*, 391.

(4) Reymond, J.-L.; Janda, K. D.; Lerner, R. A. *Angew. Chem., Int. Ed. Engl.* **1991**, *30*, 1711.

(5) Reymond, J.-L.; Janda, K. D.; Lerner, R. A. *J. Am. Chem. Soc.* **1992**, *114*, 2257.

(6) The reaction is acid catalyzed. The acid catalyst may be either hydronium ion or a general acid, for example, acetic acid (Kresge, A. J.; Chiang, Y. *J. Chem. Soc. B* **1967**, 53, 58). We have shown that the antibody-catalyzed reaction also involves rate-determining proton transfer, the direct proton source being either the hydronium ion or a carboxyl group. See ref 8.

0002-7863/94/1516-11264$04.50/0

Scheme 1. Structure of Racemic Haptens **1**–**3**, Prochiral Enol Ether Substrates **4**–**6**, Oxocarbonium Ion Intermediate **I**, and Product **7**

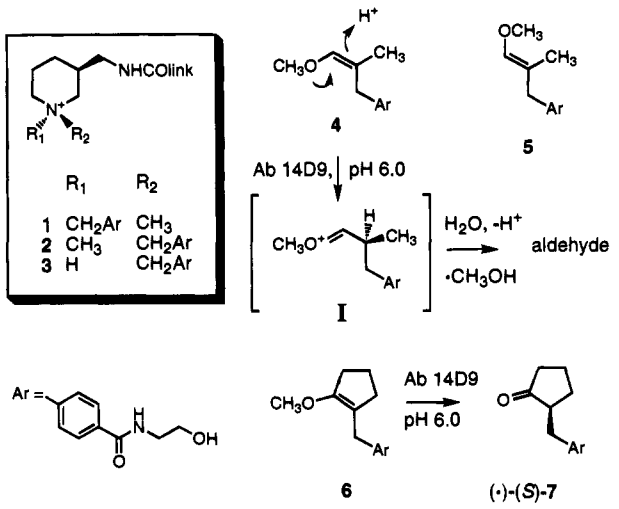

stereochemistry at the double bond and an alkyl substituent at the β-carbon undergoing protonation.[8] We have shown that antibody catalysis originates in two complementary effects: (1) general acid catalysis by an ionizable protein side chain of pK = 5.2; (2) activation of the double bond by pyramidalization, which is promoted by hydrophobic contacts complementary to the methylene substituents of the quaternary ammonium cation.

The most remarkable feature of this catalytic antibody is its very high enantioselectivity of protonation, which competes with the best existing reagents in synthesis.[9] In our effort to understand the detailed mechanism responsible for this high enantioselectivity, we now report a study of the scope of the enantioselectivity of the reaction in a set of antibodies against haptens **1** and **2**, and consider the relationship between the absolute configurations of hapten and the products. The effects of structural modifications on transition state binding are then compared with competitive inhibitions by hapten analogs. The combined results of these studies lead us to predict the structure of the antibody–transition state complex relative to the hapten, and clarify the origin of the enantioselectivity of the reaction.

Results and Discussion

Scope of Enantioselectivity in Catalysis. Antibody 14D9, anti-**1**, was originally selected as being the best catalyst among a pool of approximately 30 antibodies showing hapten-inhibited catalysis for the hydrolysis of **4**. Its exceptional properties in terms of enantioselectivity and broad substrate tolerance are its most prominent features. To test whether these were highly circumstantial, or held some relation to the structure of the hapten, we investigated the catalytic behavior of several other members of the group of anti-**1** and anti-**2** antibodies. Seven antibodies were kinetically characterized for catalysis of the hydrolysis of **4**–**6** (Table 1). The enantioselectivity of these reactions was determined for the four best catalysts of the series (Table 2). Enol ethers **4** and **5** were incubated for 5–7 days at

Table 1. Kinetic Constants for Antibody-Catalyzed Hydrolyses of Enol Ethers **4**–**6**[a]

antibody, hapten	K_M(**4**)	k_{cat}/k_{uncat}(**4**)	K_M(**5**)	k_{cat}/k_{uncat}(**5**)	K_M(**6**)	k_{cat}/k_{uncat}(**6**)
22H25, **1**	320	230	150	170	130	350
19C9, **1**	240	210	150	150	160	470
14D9, **1**	300	2500	130	290	300	10300
77E10, **2**	70	440	40	740	40	440
81C7, **2**	150	20	80	20	100	15
97C11, **2**	230	80	200	290	150	15
99C3, **2**	40	80	20	120	70	25

[a] Measured in 50 mM bis-tris buffer, pH 6.0, and 100 mM NaCl, 37 °C (**4** and **5**) or 20 °C (**6**).

Table 2. Optical Purities and Configurations of Samples Isolated from Antibody-Catalyzed Hydrolyses of Prochiral Enol Ethers **4**–**6**[a]

substrate (conditions)	antibody	conv, %	ee,[d] %	configuration[e]
4 (5 days, 37 °C)[b]	22H25	17	85	(*S*)
	19C9	14	83	(*S*)
	14D9	56	97	(*S*)
	77E10	19	79	(*S*)
5 (7 days, 37 °C)[b]	22H25	13	85	(*S*)
	19C9	15	65	(*S*)
	14D9	20	93	(*S*)
	77E10	21	82	(*S*)
6 (5 h, 20 °C)[c]	22H25	83	66	(*S*)
	19C9	82	73	(*S*)
6 (1 h, 20 °C)[c]	14D9	100	93	(*S*)
6 (20 h, 20 °C)[c]	77E10	64	49	(*S*)

[a] Solution containing 1 mM substrate and 30 μM antibody. [b] In 50 mM morpholinoethanesulfonic acid buffer, 10 mM NaCN, and 90 mM NaCl, pH 5.5. [c] In 50 mM bis-tris buffer and 100 mM NaCl, pH 7.0. [d] By ^{1}H NMR of the bis-Mosher ester of alcohol **9** or by chiral HPLC (chiralpak AS) of ketone **7**. [e] As determined by chemical correlations.[10]

Chart 1

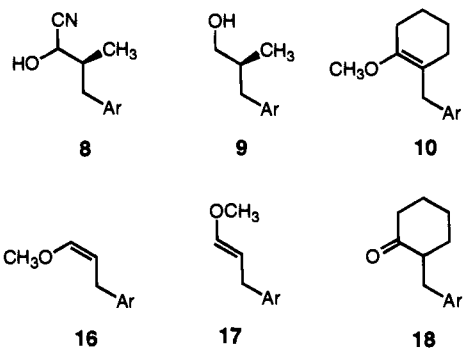

37 °C at pH 5.5 in the presence of cyanide, under which conditions the aldehyde produced is reversibly protected from racemization and oxidation as the cyanohydrin **8** (Chart 1). The enantioselectivity was determined by ^{1}H NMR on the bis-Mosher ester of the reduced alcohol **9** as described before.[5] For enol ether **6**, the reactions were conducted at pH 7 with 1 mM **6** and 30 μM antibody until the reaction significantly slowed due to product inhibition. The cyclohexanone enol ether **10** was in all cases a very poor substrate, and enantioselectivities could not be measured.

For the semipreparative catalytic hydrolysis of enol ether **6**, the reactions reached 60–90% conversion with all four catalysts. The optical enrichment in the isolated samples was correlated with the efficiency k_{cat}/k_{uncat} of the catalyst. This reflects contamination by the racemic product formed by the competing hydronium ion catalyzed hydrolysis in the medium, as well as the onset of product inhibition which further decreases the catalytic efficiency of the antibodies at high conversion ratios. The catalytic reactions taking place in the antibody combining

(7) Reymond, J.-L.; Reber, J.-L.; Lerner, R. A. *Angew. Chem., Int. Ed. Engl.* **1994**, *33*, 475.
(8) Reymond, J.-L.; Jahangiri, G. K.; Stoudt, C.; Lerner, R. A. *J. Am. Chem. Soc.* **1993**, *115*, 3909.
(9) (a) Duhamel, L.; Plaquevent, J.-C. *J. Am. Chem. Soc.* **1978**, *100*, 7415. (b) Review: Fehr, C. *Chimia* **1991**, *45*, 253. (c) Vedejs, E.; Lee, N.; Sakata, T. S. *J. Am. Chem. Soc.* **1994**, *116*, 2175 and references cited therein. (d) Matsumoto, K.; Tsutsumi, S.; Ihori, T.; Ohta, H. *J. Am. Chem. Soc.* **1990**, *112*, 9614. (e) Fehr, C.; Galindo, J. *J. Am. Chem. Soc.* **1988**, *110*, 6909. (f) Matsumoto, K.; Ohta, H. *Tetrahedron Lett.* **1991**, *32*, 4279.

Table 3. Stereoselective Inhibition of Antibody-Catalyzed Hydrolyses of Enol Ether **4**[a]

antibody	**11**	**12**	**13**	**14**
22H25	5	200	130	15
19C9	2.5	225	80	15
14D9	30	250	250	200
77E10	25	70	200	80

[a] Competitive inhibition constants K_i (μM) measured at 37 °C in 50 mM bis-tris and 100 mM NaCl at [**4**] = 100 and 300 μM and [Ab] = 2−10 μM (Ab = antibody).

Scheme 2. Synthesis of Stereochemically Defined Hapten Analogs **11**−**14**[a]

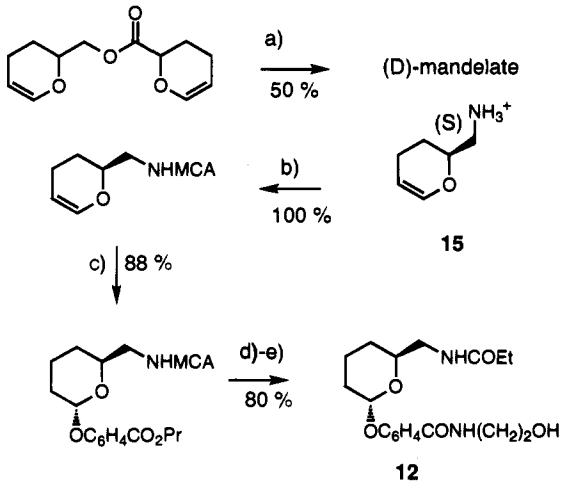

[a] Conditions: (a) NaOH, water, 20 °C, 1 h, then CH_3SO_2Cl, Et_3N, CH_2Cl_2, 0 °C, 2 h, then aqueous NH_3, acetamide, 110 °C, 15 h, then D-mandelic acid, 2-propanol/ether; (b) $(i\text{-Pr})_2EtN$, $(ClCH_2CO)_2O$, CH_2Cl_2, 0 °C, 40 min; (c) CF_3SO_3H(cat.), 4-$OHC_6H_4CO_2Pr$, CH_2Cl_2, 0 °C, 5 min, then separation by chromatography, 69% α, 18% β; (d) thiourea, 2,6-lutidine, ethanol, reflux, 1 h, then propionic anhydride, aqueous $NaHCO_3$; (e) ethanolamine, ethanol, K_2CO_3, 50 °C, 15 h.

sites are most probably completely enantioselective as is the case for 14D9. Remarkably, the four catalytic antibodies gave products of the same absolute configuration with the three substrates investigated. The absolute configuration of the products of 14D9 with **4**−**6** has been established to be (*S*) by chemical correlation,[10] so that the antibody-catalyzed protonation proceeded uniformly from the *re* face of the enol ethers.

Configuration of the Active Site. To test whether the *re* enantiofacial selectivity observed with these four catalytic antibodies held any relation to the structure of the haptens, we investigated competitive inhibition of these catalysts with the acetals **11**−**14**[4] (Table 3). These compounds are analogs of haptens **1** and **2**, and feature their essential stereochemistry, but have much lower affinity for the antibodies. Their competitive inhibition constants are in the range of 10^{-5} M and can be measured for the catalytic reaction more precisely than the very tight binding of the hapten ($<10^{-8}$ M). They were prepared in enantio- and diastereoisomerically pure form starting from a commercially available acrolein tetramer (Scheme 2). Their absolute configuration was determined by X-ray crystallography of the mandelate **15** used to resolve the enantiomers.

The results of the competitive inhibition of the antibody-catalyzed hydrolysis of **4** are shown in Table 3 and Figure 1. A

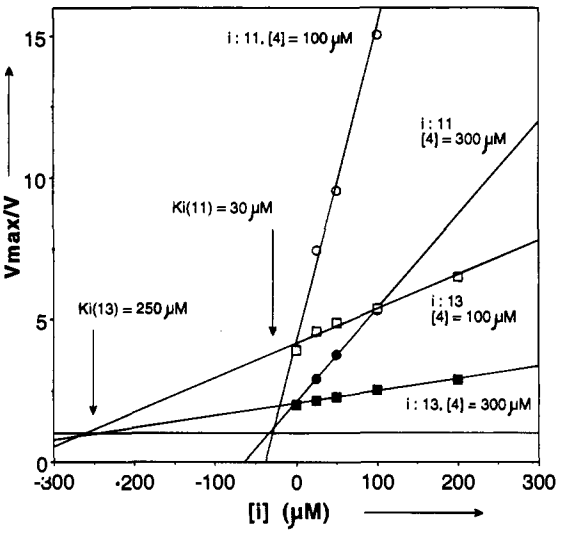

Figure 1. Dixon plot for competitive inhibition of antibody 14D9 catalyzed hydrolysis of **4** by stereochemically pure hapten analogs **11** (2*S*,6*R*) and **13** (2*S*,6*S*) (Table 3) in 50 mM bis-tris, pH 6.0, and 100 mM NaCl, 37 °C. For each inhibitor, the lines obtained with [**4**] = 100 μM and [**4**] = 300 μM cross on the horizontal line of $1/V_{max}$. The coordinate of this intersection point on the [i]-axis gives $-K_i$.

clear selectivity was observed for the (*R*)-α-stereoisomer **11** with all four antibodies. This provides strong evidence that these antibodies are stereospecifically binding the corresponding (*S*,*S*) isomer of hapten **1** with the benzyl substituent in the axial position.[4] This is somewhat surprising in the case of antibody 77E10, which was raised against the equatorial hapten isomer **2**. This hapten was however only 95% diastereoisomerically pure and provided a much weaker immune response than **1**. The inhibition pattern of antibody 77E10 with hapten analogs **11**−**14** suggests that its active site is complementary to **1**, and that this antibody was therefore part of the immune response directed against the 5% contaminant **1** in hapten **2**.

Analysis of the Transition State. At that point, we became interested to understand the exact orientation of the enol ether function at the transition state in the antibody active site, relative to the hapten, which, if unique and common to all antibodies, could explain the observed correlation between the absolute configurations of hapten and the products. We concentrated our efforts on the 14D9 catalyst, the fastest and best understood antibody of the series. The following assumptions were taken concerning antibody−substrate binding and transition state structure.

(1) The aromatic group is a fixed anchoring point common to all substrates and haptens entering the active site. We have demonstrated previously that modification of this group leads to a dramatic reduction in affinity, implying that binding to this functional group in very strong.[4]

(2) The transition state of the protonation reaction is late for all substrates and may be approximated by the protonated oxocarbonium ion intermediate **I** (Scheme 1), where the β-carbon atom of the enol ether essentially adopts a tetrahedral (sp^3) geometry. Solvent kinetic isotope effects[11] and Bronsted coefficients[12] show that carbon−hydrogen bond formation is approximately two-thirds complete at the transition state for protonation by the hydronium ion or carboxylic acids. We have established that the same applies for the catalytic reaction of **4** within the antibody active site.[8]

(10) (a) Alcohol (*S*)-**9** has been prepared enantiospecifically by alkylation of Evan's propionate with methyl 4-(bromomethyl)benzoate. Shabat, D.; Itzhaky, H.; Reymond, J.-L.; Keinan, E. Submitted for publication. (b) Reference 9d.

(11) Kresge, A. J.; Sagatys, D. S.; Chen, H. L. *J. Am. Chem. Soc.* **1977**, *99*, 7228.

(12) Kresge, A. J.; Chen, H. L.; Chiang, Y.; Murrill, E.; Payne, M. A.; Sagatys, D. S. *J. Am. Chem. Soc.* **1971**, *93*, 413.

Chart 2. Transition State Structures for Protonation of **4** on the *re* Face in a Chiral Active Site Complementing (*S,S*)-**1**

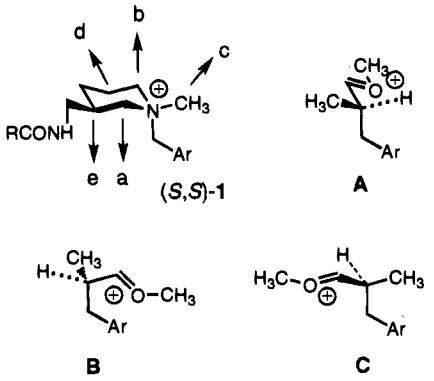

Table 4. Dissociation Constants of Antibody−Substrate (K_M) and Antibody−Transition State (K_{TS}) Complexes for 14D9-Catalyzed Hydrolyses of Enol Ethers (Data from Reference 8)

	pH, *T*, °C	K_M, μM	k_{cat}, s^{-1}	k_{uncat}, s^{-1}	k_{cat}/k_{uncat}	K_{TS}, nM
4	5.5, 37	340	9.5×10^{-5}	3.8×10^{-8}	2500	135
4	5.9, 20	150	1.6×10^{-5}	2.3×10^{-9}	7000	20
5	5.5, 37	130	8.3×10^{-6}	2.9×10^{-8}	290	450
6	7.0, 20	315	5.4×10^{-2}	4.2×10^{-6}	12500	25
6	6.0, 20	300	3.9×10^{-1}	3.8×10^{-5}	10250	30
10	7.0, 20	370	8.8×10^{-5}	2.4×10^{-7}	370	1000
16	5.9, 37	250	6.2×10^{-5}	3.5×10^{-7}	180	1400
16	6.1, 20	200	1.9×10^{-5}	3.2×10^{-8}	600	330
17	5.9, 37	240	4.0×10^{-6}	3.8×10^{-8}	180	1300

(3) The methyl or methylene groups attached to the β-carbon of the enol ether are tightly bound in the transition state. These substitutents increase the catalytic effect of antibody 14D9 by a factor of 100 without affecting ground state binding.[8] This may be explained by activation of the double bond through a geometrical strain effect mediated by hydrophobic interactions between these groups and the binding site complementary to the quaternary ammonium hapten.[4]

Following these assumptions, three possible transition state structures can account for the enantioselective protonation on the *re* face of the enol ether in the active site complementary to (*S,S*)-**1** (Chart 2). Structure **A**, which assumes proton delivery from the direction of the methyl group, could be suggested by the observation that cyclic substrates are tolerated, and by direct analogy to the piperidine hapten **3**, which also produced catalysts, and where the NH bond mimics the proton transfer. Structures **B** and **C** assume that the β-methyl group of the substrate binds to the antibody site complementary to either the other side of the piperidine cycle (b), or the *N*-methyl substituent itself (c), a possibility that can not be ruled out *a priori*.

Methyl substitution in position β increases catalysis by a factor of 12.[8] Furthermore, the cyclopentanone enol ether **6** (Scheme 1) was an excellent substrate, while the cyclohexanone enol ether **10** (Chart 1) was very poor. These substrates all bound the antibody with similar affinities (K_M, Table 4), so that nonproductive substrate binding could not account for these effects on catalysis.[13] Fitting these substrates onto the (*S,S*)-hapten **1** as in **A** rather suggested that the six-membered ring substrate would be either tightly bound or a better substrate. Alternative structure **B** or **C**, although unusual in that the cyclic substrates would have to occupy space not "allowed" within the hapten structure, should therefore also be considered.

Inhibition by Hapten Analogs. To test if the alternative structures **B** and **C** might be accessible to the transition states

Table 5. Structures and Competitive Inhibition Constants of Antibody 14D9 (Anti-**1**) Catalyzed Hydrolysis of Enol Ether **4** for Alkylammonium Cations

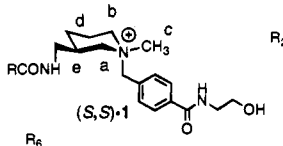

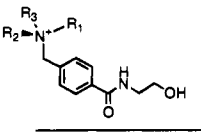

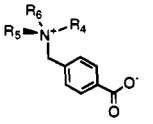

	R_1	R_2	R_3	K_i, μM
19	H	H	H	450
20	CH_3	H	H	55
21	CH_3	CH_3	H	5

	22	**23**	**24**	**25**	**26**
R_4	CH_3	CH_3	CH_3	CH_3	CH_2CH_3
R_5	CH_3	CH_3	CH_3	CH_2CH_3	CH_2CH_3
R_6	H	CH_3	CH_2CH_3	CH_2CH_3	CH_2CH_3
K_i, μM	200	18	7	7	40

	27	**28**	**29**
R_4	CH_3	H	CH_3
R_5	CH_2CH_3	CH_2CH_3	$(CH_2)_2CH_3$
R_6	H	CH_2CH_3	H
K_i, μM	60	40	30

Table 6. Structures and Competitive Inhibition Constants of Antibody 14D9 Catalyzed Hydrolysis of Enol Ether **4** for Pyrrolidium and Piperidinium Cations

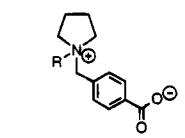

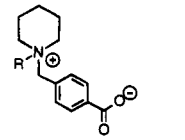

	R	K_i, μM		R	K_i, μM
30	H	50	**34**	H	100
31	CH_3	2.5	**35**	CH_3	0.9
32	CH_2CH_3	8	**36**	CH_2CH_3	7
33	$(CH_2)_2CH_3$	7	**37**	$(CH_2)_2CH_3$	13

of the cyclic substrates **6** and **10** within the antibody active site, it was first necessary to probe the energetics of binding and the availability of the space complementing the ammonium center of the hapten in the antibody active site. This was accomplished by investigating competitive inhibition of the 14D9-catalyzed hydrolysis of **4** with a series of alkyl-substituted benzylammonium cations analogous to the hapten.

Compounds **19**−**37** were synthesized by alkylation of 4-(chloromethyl)benzoic acid or *N*-(hydroxyethyl)-4-(chloromethyl)-benzamide with an excess of the corresponding amines, and purified by preparative HPLC as their trifluoroacetate (TFA) salts. Competitive inhibition of the 14D9-catalyzed hydrolysis of **4** (100 and 300 μM) at pH 6.0 and 37 °C was observed for all of these compounds (Tables 5 and 6).

The affinity of antibody 14D9 for the amine **19** increases by a factor of 10 for the addition of the first and second methyl groups. At the stage of tertiary amine **21**, binding becomes too tight to be accurately measurable by competitive inhibition, because the binding constants approach the concentration of

(13) Nonproductive substrate binding in the active site can be considered as competitive inhibition by the substrate. It behaves kinetically like the case of substrate contamination by an endogeneous competitive inhibitor. In this situation, both K_M and k_{cat} are decreased by the same factor (the Line-weaver Burke plot gives a line parallel to but higher than the line without inhibitor). Therefore, any reduction in the apparent k_{cat} induced by nonproductive binding must also appear in a comparably tighter binding of the substrate. This is obviously not the case with the cyclic enol ethers **6** and **10** which have comparable K_M values. Segel, I. H. *Enzyme Kinetics;* John Wiley & Sons: New York, 1993; pp 147−148.

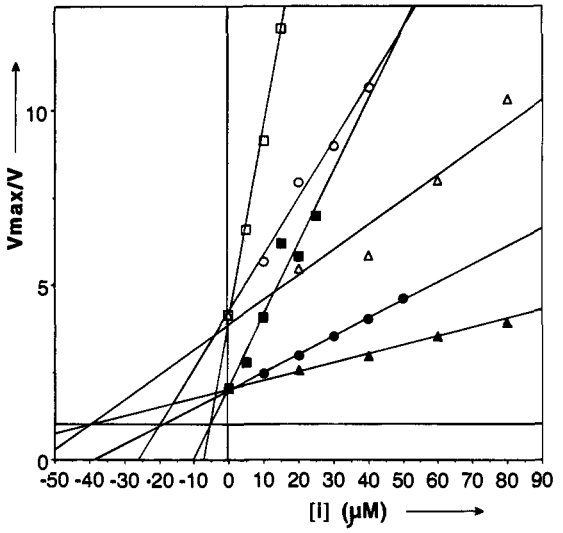

Figure 2. Dixon plot for competitive inhibition of antibody 14D9 catalyzed hydrolysis of enol ether **4** by quaternary (4-carboxybenzyl)-ammonium cations (Table 5) in 50 mM bis-tris, pH 6.0, and 100 mM NaCl, 37 °C: **23** (trimethyl) with [**4**] = 100 μM (○) and 300 μM (●); **25** (diethylmethyl) with [**4**] = 100 μM (□) and 300 μM (■); **26** (triethyl) with [**4**] = 100 μM (△) and 300 μM (▲). For each inhibitor, the lines obtained with [**4**] = 100 μM and [**4**] = 300 μM cross on the horizontal line of $1/V_{max}$. The coordinate of this intersection point on the [i]-axis gives $-K_i$.

antibody present in the experiment (2 μM). Fortunately, the affinity of these inhibitors can be reduced 50-fold by substitution of the *N*-hydroxyethanecarboxamide with a carboxylate, allowing the study of further substitution. Addition of a third methyl group on **22** to give the quaternary ammonium salt **23** again increases the affinity by a factor of 10. Thus, strong binding interactions of the same magnitude exist between the antibody and the methyl and methylene groups in the first sphere of the quaternary ammonium center. The gain in binding energy for each additional methyl group is similar to the difference in the dissociation constants K_{TS} (see below) for the transition states of protonation with enol ethers **16** and **4**, which also differ by a single methyl group at that position. Significantly, no functional group on the antibody forms an energetically favorable hydrogen bond with the protonated amines, which should have made the tertiary amines **21** and **22** the tightest binders of the series. This provides further evidence that the general acid responsible for catalysis in the antibody active site does not act as a direct proton shuttle to the double bond of the enol ether.[8]

Binding in the second sphere of methylene groups is revealed by the substitution of ethyl for methyl groups (Figure 2, Table 5). The first substitution (**23** to **24**, **22** to **27**) increases the affinity by a factor of 2, and the second (**24** to **25**, **27** to **28**) has no effect at all on binding, but the third substitution (**25** to **26**) decreases the affinity by a factor of 5. These effects can be readily interpreted by inspection of the structure of hapten **1**. The 2-fold gain in the first substitution can be attributed to binding at the methylene site d. The second substitution would fill site e, which is complementary to a tertiary carbon atom and might indeed not provide much binding to a methyl group. The third substitution forces one methyl group out of the space allowed by the hapten structure, and causes a steep decrease in affinity.

Further confirmation of these substitution effects is provided by the competitive inhibition constants K_i of the cyclic amines **30**–**37** (Table 6). N-methylation of the piperidine derivative **34** to give the ammonium salt **35**, which is most congruent to the original hapten, dramatically increases the affinity by a factor of 100. Ethylation (**35** to **36**) results in a 10-fold decrease in binding. A similar but less extreme trend is seen with the pyrrolidine derivatives **30**–**32**.

Chart 3. Free Energy Diagram for Antibody Binding to the Substrate and Transition State

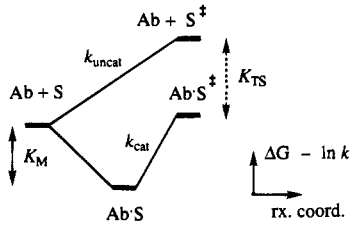

These inhibition experiments with hapten analogs demonstrated that additional methylene substituents could be installed in the space not allowed by the structure of the hapten at a reasonable energetic cost, and pointed to the possibility that the transition state structures **B** and **C** (Chart 2) might be accessible.

Competitive Inhibition and Transition State Binding. The hapten and close derivatives of it are in essence transition state analogs of the reaction. If a transition state analog binds to the antibody in the same orientation as the real transition state of protonation, equivalent substitutions should have the same influence on its affinity as on catalysis. These effects can be evaluated quantitatively as follows. The Michaelis–Menten constant K_M gives a measure of the equilibrium among the substrate, antibody, and antibody–substrate complex (eq 1). The

$$Ab{\cdot}S \overset{K_M}{\rightleftharpoons} Ab + S \qquad K_M = [Ab][S]/[Ab{\cdot}S] \qquad (1)$$

dissociation constant K_{TS}, which measures the equilibrium among the transition state of the reaction in solution, the antibody, and the antibody–transition state complex, is given by $K_{TS} = K_M/(k_{cat}/k_{uncat})$ (Chart 3, eq 2). K_{TS} is the dissociation

$$Ab{\cdot}S^{\ddagger} \overset{K_{TS}}{\cdots\!\rightarrow} Ab + S^{\ddagger} \qquad K_{TS} = K_M k_{uncat}/k_{cat} \qquad (2)$$

constant for the antibody–transition state complex, and gives a direct measure of the affinity of the catalytic antibody for the transition state of the reaction, or catalysis. Finally, using any substrate as the catalytic probe, the competitive inhibition constant K_i for a given inhibitor reflects the equilibrium among the inhibitor, the antibody, and their complex, in the absence of substrate (eq 3).[14] K_M, K_{TS}, and K_i reflect equivalent

$$Ab{\cdot}i \overset{K_i}{\rightleftharpoons} Ab + i \qquad K_i = [Ab][i]/[Ab{\cdot}i] \qquad (3)$$

equilibria between species in solution and the antibody, and may therefore be used to compare inhibition by transition state analogs with catalysis.

Structure of the Antibody–Transition State Complex. By inspecting the results obtained with the series of hapten analogs above (Tables 5 and 6), it became evident that the effect of the substitution of ethyl for methyl at the β-carbon of the enol ether on catalysis, as measured by the dissociation constants K_{TS}, would provide a definitive distinction among the transition state structures **A**–**C** (Chart 2). The trend observed in the competitive inhibition constants of the methyl- and ethyl-substituted ammonium ions leads to the following predictions: if the transition state orientation was as in **A**, where the additional methyl group would bind site a in the transition state, **4** and its β-ethyl analog would be hydrolyzed with similar efficiencies,

(14) Segel, I. H. *Enzyme Kinetics*; John Wiley & Sons: New York, 1993; pp 109–111.

Table 7. β-Substituted Enol Ethers: Structures and Kinetic Parameters for Background[a] and Antibody 14D9[b] Catalyzed Hydrolyses

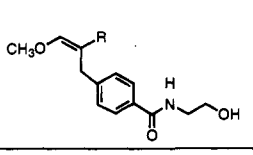

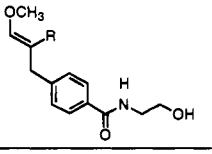

	16 (R = H)	**4** (R = CH_3)	**38** (R = CH_2CH_3)	**17** (R = H)	**5** (R = CH_3)	**39** (R = CH_2CH_3)
k_{uncat}, s^{-1}	3.5×10^{-7}	3.8×10^{-8}	2.3×10^{-8}	3.8×10^{-8}	2.9×10^{-8}	2.1×10^{-8}
k_{cat}, s^{-1}	6.2×10^{-5}	9.5×10^{-5}	4.2×10^{-6}	4.0×10^{-6}	8.3×10^{-6}	1.8×10^{-6}
K_M, μM	250	340	550	240	130	150
K_{TS}, nM	1400	140	3000	1300	450	1830

[a] k_{uncat} is the apparent first-order rate constant for hydrolysis of the enol ether in bis-tris buffer (50 mM) and 100 mM NaCl, pH 5.5 (**4** and **5**), 5.9 (**16** and **17**) or 5.8 (**38** and **39**), 37 °C. [b] k_{cat} is the apparent first-order rate constant for reaction of the antibody–substrate complex under the same conditions. Both reactions are first order in hydronium ion above pH 5.5; see ref 8.

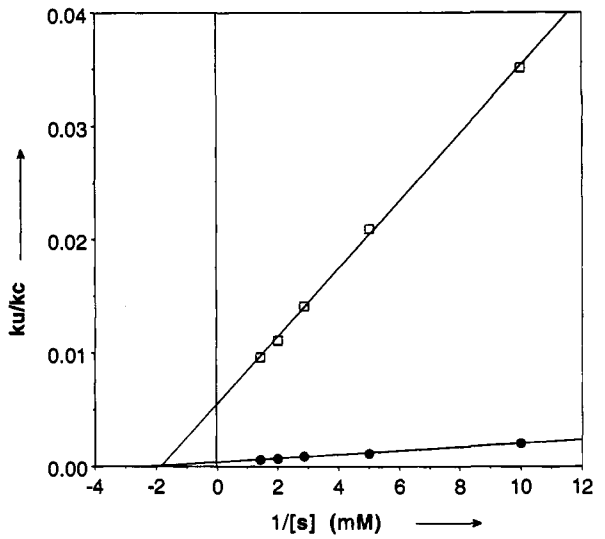

Figure 3. Double reciprocal plot of initial rates as ($k_{uncat}/k_{cat\ app}$) vs 1/[S] for antibody 14D9 catalyzed hydrolysis of (●) **4** and (□) **38**, measured in 50 mM bis-tris, pH 6.0, 100 mM NaCl, 37 °C, and 2 or 6 μM antibody 14D9. K_{TS} is given by the slope of the lines and $1/K_m$ by the negative intercept on the 1/[S]-axis. See text.

in analogy to the binding of quaternary ammonium cations **24** and **25**; for **B**, substitution of ethyl for methyl should result in tighter transition state binding, and thus increased catalysis, by filling site b, in analogy to the increased binding of **25** compared to **24**; finally, structure **C** would result in a decrease in catalysis by forcing the additional methyl group out of the allowed space, in analogy to the drop in affinity seen from **25** to **26** (5-fold), **31** to **32** (3-fold), and **35** to **36** (7-fold).

The ethyl substituted enol ethers **38** and **39** were synthesized as described before for the methyl compounds **4** and **5**,[8] starting from 2-methylene-1-butanol, and separated by preparative HPLC. Catalysis by antibody 14D9 for the hydrolysis of these compounds was assayed at 37 °C, pH 6. Both **38** and **39** were catalytically hydrolyzed by antibody 14D9, but with only very modest rate enhancements (Table 7). For **38**, $k_{cat}/k_{uncat} = 180$ compares to $k_{cat}/k_{uncat} = 2500$ for the methyl compound **4** under these conditions (Figure 3), and $k_{cat}/k_{uncat} = 84$ for **39** compares with $k_{cat}/k_{uncat} = 290$ for **5**. Thus, for both the (*E*)- and the (*Z*)-enol ethers, substitution of ethyl for methyl at the β-carbon causes a steep drop in transition state binding. As was the case for the five- and six-membered ring enol ethers **6** and **10**, substrate binding is weaker for the poorer substrates, so that the decrease in rate enhancement cannot be caused by nonproductive binding.[15]

This substitution experiment provides conclusive evidence that the transition state in the antibody 14D9-catalyzed enantioselective protonation fits structure **C** (Chart 2). This evidence is substantiated by the correlation of absolute configurations of hapten and the products, as well as by the inhibition studies above which document the energetics of binding in the antibody active site. In structure **C**, the substituent of the β-carbon atom is bound to the site corresponding to the *N*-methyl group of hapten **1**. Extension of one methylene group at that site places the substituent out of the space allowed within the structure of the hapten, and results in a sharp drop in catalysis. This effect parallels the effect of the addition of an ethyl group in the series of ammonium ions **25**, **26**, **31**, **32**, and **35**, **36**.

The exceptional situation with the cyclopentanone enol ether **6**, which is an excellent substrate (Table 4), is also reproduced in the 5-fold difference in affinity between the ethylpyrrolidinium **32** and the triethylammonium cation **21**. This suggests that **32** might bind to the active site with its ring as in **C**, where the five-membered ring transition state and inhibitors would find themselves in an energetically favorable situation not accessible to either the ethyl or cyclohexyl transition states. The weak transition state binding observed for the hydrolysis of **10** (K_{TS} = 1000 nM) relative to **6** (K_{TS} = 25 nM), by 14D9, is not reproduced by a similar difference in inhibition constants between the quaternary piperidinium cations **35**–**37** and the pyrrolidinium cations **31**–**33** (Table 6). This suggests that **35**–**37**, unlike **31**–**33** which seem to bind as in **C** (see above), bind the antibody as in **A**, which is probably most favorable for these close analogs of the hapten.

For the (*E*)-enol ethers, the effect of the substitution of ethyl for methyl at the β-carbon on transition state binding by the antibody, $K_{TS}(\mathbf{39})/K_{TS}(\mathbf{5}) = 4$, is comparable to the effects seen in the inhibition constants of the corresponding ammonium cations. Remarkably, these structural effects on antibody catalysis are significantly larger with the (*Z*)-enol ethers:[15] $K_{TS}(\mathbf{38})/K_{TS}(\mathbf{4}) = 20$ for substitution of ethyl for methyl, and $K_{TS}(\mathbf{10})/K_{TS}(\mathbf{6}) = 40$ (Table 4) for the difference between six- and five-membered rings. The existence of such large effects on catalysis may reflect the fact that, as being energy maximums with insignificant lifetimes, antibody–transition state complexes cannot relax by small adjustments to accommodate unfavorable binding interactions, as can the stable antibody–inhibitor complexes.

Origin of the Enantioselectivity. Having elucidated the stereochemical and conformational relationship between hapten and the transition state, a more detailed understanding of the

(15) This was already the case for the effect of methyl for hydrogen substitution, which results only in a 3-fold decrease in K_{TS} between **17** and **5** as compared to a 10-fold effect between **16** and **4**. A significant difference between (*Z*) and (*E*) isomers exists only in the β-methyl-substituted compounds **4** and **5**. As discussed in ref 8, hydrophobic interactions between the antibody and the β-carbon substituent can account for this situation, by being directed almost exclusively to transition state binding in **4** and partly to substrate binding in **5** (Table 7).

Chart 4. Competitive Inhibition of 14D9-Catalyzed Hydrolysis of **4** by Enantiomerically Pure Reaction Products **7** and **18**

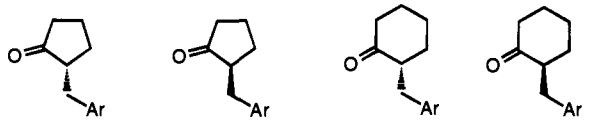

(+)-(*R*)-**7**	(-)-(*S*)-**7**	(+)-(*R*)-**18**	(-)-(*S*)-**18**
K_i = 100 μM	K_i = 100 μM	K_i = 100 μM	K_i = 50 μM

origin of the enantioselectivity in the antibody-catalyzed reaction could now be envisioned. We investigated the possibility that both catalysis and enantioselectivity might be reproduced in the binding of the reaction products **7** and **18**. These can be considered as neutral transition state analogs as their geometry resembles the fully protonated oxocarbonium ion intermediates formed in the rate-determining protonation step.

Samples of ketones **7** and **18** (Scheme 1 and Chart 1) were resolved by HPLC (chiracell AS), and the absolute configuration of the pure enantiomers was assigned on the basis of their optical rotation. Competitive inhibition of the 14D9-catalyzed hydrolysis of **4** was assayed at 37 °C and pH 6 for 48 h, under which conditions these compounds were enantiomerically stable (<2% racemization as estimated by HPLC). Remarkably, no significant binding selectivity was observed among these four compounds, their competitive inhibition constants K_i being almost equal (Chart 4). Not only was the 40-fold preference for the five-membered ring over the six-membered ring transition state totally absent, but there was no enantioselectivity at all on binding of the enantiomers of ketone **7** despite the very high enantioselectivity of the antibody-catalyzed reaction in favor of (*S*)-**7**.

Although the enantiomers of **7** and **18** do not possess the methyl substituent of the oxocarbonium ion and their binding is less constrained than in the antibody–transition state complex,[16] one would have expected at least some degree of selectivity, as seen above with the binding of the quaternary ammonium ions. This lack of selectivity rather resembles the binding of antibody 14D9 with the five- and six-membered ring substrates **6** and **10** (Table 4), pyrrolidine **30**, and piperidine **34** (Table 6). We propose that binding of these compounds in the antibody active site involves an equilibrium among orientations corresponding to **A**–**C** (Chart 2) and that the singular selectivity observed for the transition state leading to (*S*)-**7** appears because it is constrained to structure **C**. As this constraint applies only to the transition state, it represents most probably a predetermined direction of proton delivery in the antibody active site, which is imposed by the position of the antibody side chain assisting protonation by general acid catalysis.[8] Alignment with the general acid residue, even if it might be sometimes favorable, should indeed not be a strict constraint for the binding of substrates, products, or inhibitors in the antibody active site.

As seen above with the effect of increasing methyl substitution at the ammonium center on affinity (**19**–**21**, **22**–**23**, Table 5), the *N*-methyl and both methylene groups adjacent to the nitrogen of the piperidine ring are bound with similar affinities (sites a–c, Chart 2). Activation of the double bond by pyramidalization should be as effective in structures **A**–**C**. Having imposed the direction of proton delivery as in **C** (Chart 2), switching the methyl and oxocarbonium substituents at the β-carbon, to give the diastereoisomeric structure leading to the (*R*) enantiomer, should still allow productive hydrophobic contacts in site a for double bond activation. The observed exclusive preference for the (*S*) transition state may be a dual effect involving selective stabilization of the oxocarbonium ion in site a by the general acid, and exclusion of this group from the N-methyl site c for the same reasons underlying the drop in catalysis from **4** to **38** and **5** to **39** (Table 7).

Implications for the Reaction Mechanism. As we have seen, the antibody active site complementing the ammonium center of hapten **1**, where protonation occurs, is surrounded in all directions by hydrophobic binding sites to its alkyl substituents. It means that the proton, which is delivered from direction b (Chart 2), has to cross a hydrophobic region of the protein to reach the β-carbon of the enol ether. By a correlation of solvent kinetic isotope effects on the hydrolysis of a series of enol ethers using the Marcus rate theory, Kresge et al. have shown that a significant part of the activation energy for enol ether protonation involves desolvation of the acid catalyst.[13] Desolvation of the proton source in the hydrophobic environment of the antibody active site could significantly contribute to catalysis.

Earlier evidence from substrate variations[8] as well as the inhibition experiments above suggests that the general acid residue implicated in the antibody-catalyzed protonation of enol ethers might not act as a direct proton shuttle, but rather in the stabilization of the oxocarbonium ion intermediate. In any case, this group should be in line with the carbon–hydrogen bond being formed and/or the π* orbitals of the oxocarbonium ion. According to our model of the transition state, it should be found within the plane defined by the nitrogen atom and the two adjacent methylene groups of the piperidine ring in the hapten, in close proximity to site a or b (Chart 2). One possibility would be that the general acid forms a hydrogen bond with the NH of the amide linker in the antibody–hapten complex, which would explain the existing correlation between the *re* enantioselectivity of protonation and the (*S*,*S*) configuration of the hapten.

Conclusion

Substrate tolerance and enantioselectivity in the antibody-catalyzed hydrolysis of enol ethers have been shown to be recurrent features in a series of anti-**1** and anti-**2** antibodies. Four antibodies were shown to produce (*S*)-configured reaction products from three different, prochiral enol ethers. These four antibodies also stereoselectively bound hapten analog **11**, showing that their active site was complementary to the corresponding (*S*,*S*) stereoisomer of hapten **1**. Further experiments will be needed to see if immunization with optically pure hapten **1** allows catalytic antibodies of predictable enantiofacial selectivity of protonation to be produced.[17]

In the case of antibody 14D9, a systematic study of the effects of structural variations on catalysis and inhibition leads to the prediction of structure **C** (Chart 2) for the transition state of protonation in the antibody active site. Most significantly, the structure of the antibody–transition state complex turned out not to be following the simplest interpretation of the hapten structure.

The origin of the very high enantioselectivity of protonation of prochiral enol ethers by antibody 14D9 could be attributed to three constraints on the reaction: (a) substrate binding at the aromatic benzamide group, (b) general acid catalysis by a localized protein side chain, (c) productive binding of the

(16) Hyperconjugation of the carbon–hydrogen bond being formed with the π*-orbitals of the oxocarbonium ion imposes a strict constraint on the conformation of the transition state, which does not apply to the products. Furthermore and as mentioned above, the antibody–transition state complex does not have a lifetime, and therefore cannot accomodate unfavorable interactions by small conformational adjustments.

(17) Ikeda, S.; Weinhouse, M. I.; Janda, K. D.; Lerner, R. A.; Danishefsky, S. J. *J. Am. Chem. Soc.* **1991**, *113*, 7763.

β-carbon's alkyl substituent to the *N*-methyl site at the transition state and exclusion of the oxocarbonium ion from this site for steric or electronic reasons. The binding selectivity of antibody 14D9 for the enantiomeric transition states did not appear in the binding of the enantiomeric products despite their close structural resemblance to the transition state. These experiments provide a clear and quantitative illustration that binding transition states rather than ground state molecules can provide a decisive advantage in terms of enantioselectivity, and suggest that antibodies are indeed extremely well suited for enantioselective catalysis.

Analysis of the antibody−transition state complex was possible because its dissociation constant (K_{TS}) can be deduced directly from the kinetic constants of the reaction, and compared with competitive inhibition constants of transition state analogs, providing quantitative information on an elusive species that does not have a lifetime because it represents an energy maximum. This information is not accessible otherwise, and should be combined with structural analysis of stable antibody−substrate, antibody−product, or antibody−inhibitor complexes[18] to yield a complete picture of the antibody 14D9-catalyzed reaction.

Experimental Section

A. Synthesis. General Remarks. Reagents were purchased from Aldrich or Fluka. Solvents were ACS grade from Fisher. All chromatographies (flash) were performed with Merck Silicagel 60 (0.040−0.063 mm). Preparative HPLC was done using Fisher Optima grade acetonitrile and ordinary deionized water. TLC was performed with fluorescent Merck F254 glass plates. NMR spectra were recorded on a Bruker AM-300 MHz or AM-500 MHz instrument. The chemical shift δ is given in parts per million and the coupling constant ^3J or ^2J in hertz. Solvent was used as the reference as $\delta(CHCl_3) = 7.27$, $\delta(CHCl_3) = 77.0$, $\delta(DHO) = 4.80$, and $\delta(CH_3COCH_3$ in $D_2O) = 29.8$. MS, HRMS (high-resolution mass spectra), and combustion analyses were provided by the Scripps Research Institute facility (Gary Suizdak). X-ray crystallography was provided by Dr. Raj K. Chadha at the Department of Chemistry, The Scripps Research Institute.

3,4-Dihydro-2*H*-pyran-2-methanamine, l- and d-**Mandelic Acid Salts 15.** A solution of (3,4-dihydro-2*H*-pyran-2-yl)methyl 3,4-dihydro-2*H*-pyran-2-carboxylate (29 g, 0.13 mol) and sodium hydroxide (5.7 g, 0.15 mol) in 100 mL of water was stirred at 20 °C for 1 h, then poured into aqueous saturated $NaHCO_3$, and extracted with CH_2Cl_2 (7 × 60 mL). After removal of the solvent, the crude 3,4-dihydro-2*H*-pyran-2-methanol was dissolved in 0.4 L of dry CH_2Cl_2 and treated at 0 °C with 20 mL of triethylamine (0.15 mol) and 10 mL of methanesulfonyl chloride (0.13 mol). After 2 h at 0 °C, the reaction was poured into aqueous saturated $NaHCO_3$ and extracted with CH_2Cl_2 to give (3,4-dihydro-2*H*-pyran-2-yl)methyl methanesulfonate (25.6 g, 0.13 mol, 100%), which was then dissolved in 28% NH_3 in water (0.35 L) and acetamide (200 g) as cosolvent and heated in several small pressure reactors (40 mL each) at 110 °C for 15 h. The solution was then diluted with 200 mL of water and 150 mL of NaOH (1 N), and extracted with CH_2Cl_2 (15 × 100 mL). After concentrating the extracts to 300 mL, the solution of the crude amine was treated with L-(+)-mandelic acid (15.2 g, 0.1 mol). The solvent was then completely removed and the residue diluted with 2-propanol (50 mL). Addition of excess diethyl ether induced crystallization, giving 17 g (64 mmol, 50%) of **15**. Six successive recrystallizations, induced by slow cooling of solutions saturated in refluxing 2-propanol, gave 2.5 g of diastereomerically pure (>97% diastereomeric excess (de)) L-mandelate of **15**. The combined mother liquors were dissolved in 150 mL of NaOH (1 N), extracted with CH_2Cl_2 (7 × 80 mL), and treated as above with 12 g of D-(−)-mandelic acid. Five recrystallizations gave 3.6 g of diastereomerically pure D-mandelate of **15** (97% de). Crystals suitable for X-ray analysis were obtained from a 2-propanol/ether solution of this salt left standing at 20 °C for 2 months.

Data for (*R*)-3,4-dihydro-2*H*-pyran-2-methanamine, (*S*)-mandelic acid salt ((+)-**15**): colorless solid; mp 124−5 °C; $\alpha_D = +5.7$ ($c = 2$, EtOH); ^{1}H NMR (500 MHz, D_2O) δ 7.44−7.38 (m, 5H), 6.41 (br d, 1H, $J = 6$), 5.00 (s, 1H), 4.90 (m, 1H), 4.80 (s, 3H), 4.13 (tt, 1H, $J = 9$, 1.5), 3.19 (dd, 1H, $J = 13$, 3), 3.14 (dd, 1H, $J = 13$, 9), 2.09 (m, 1H), 2.02 (m, 1H), 1.93 (m, 1H), 1.66 (m, 1H); ^{13}C NMR (125 MHz, D_2O) δ 166.7, 129.3, 127.9, 116.2, 115.6, 114.4, 89.7, 62.3, 58.3, 17.6, 11.5, 5.4. Anal. Calcd for $C_{14}H_{19}NO_4$ (265.3): C, 63.38; H, 7.22; N, 5.28. Found: C, 63.53; H, 7.24; N, 5.30.

2-[4′-[*N*-(Hydroxyethyl)carbamyl]phenoxy]-6-(propanamidomethyl)tetrahydropyrans 11 (2*S*,6*R*), 12 (2*R*,6*S*), 13 (2*R*,6*R*), and 14 (2*S*,6*S*). *N*,*N*-diethylisopropylamine (0.5 mL) was added to a suspension of 0.5 g (1.9 mmol) of diastereoisomerically pure L-mandelate **15**, which dissolved after 15 min at 20 °C. The solution was then cooled to 0 °C and treated with 490 mg of chloroacetic anhydride. Chloroacetylation was complete after 40 min at 0 °C. The solution was poured into phosphate buffer, pH 7, and extracted with CH_2Cl_2. Removal of the solvent yielded 365 mg (100%) of optically pure *N*-((2*R*)-3,4-dihydro-2*H*-pyran-2-ylmethyl]chloroacetamide as a crystalline solid, $\alpha_D = -58°$ ($c = 0.8$, EtOH). This compound was then dissolved in 20 mL of anhydrous CH_2Cl_2. Powdered 3A molecular sieves (0.5 g) freshly activated by flame-drying under vacuum and 1.1 g (6 mmol) of propyl 4-hydroxybenzoate were added. The solution was cooled to 0 °C under argon, and 2 drops of trifluoromethanesulfonic acid was added. The reaction was complete after 5 min at 0 °C and quenched by addition of 5 drops of triethylamine, poured into phosphate buffer, pH 7, and extracted with CH_2Cl_2. Chromatography of the residue on silica gel (150 g, ether/hexane (1:1)) gave (2*S*,6*R*)-2-[4′-[(carboxypropyl)oxy]phenoxy]-6-[(chloroacetamido)methyl]tetrahydropyran ($R_f = 0.15$; 480 mg, 1.23 mmol, 69%; mp 100−100.5 °C. Anal. Calcd for $C_{18}H_{24}NO_5Cl$ (369.88): C, 58.45; H, 6.54; N, 3.79. Found: C, 58.01; H, 6.49; N, 3.72, and (2*R*,6*R*)-2-[4′-[(carboxypropyl)-oxy]phenoxy]-6-[(chloroacetamido)methyl]tetrahydropyran ($R_f = 0.10$; 125 mg, 0.34 mmol, 18%; mp 126−127 °C. Found: C, 57.89; H, 6.44; N, 3.69).

A solution of the (2*S*,6*R*) isomer (50 mg) with thiourea (20 mg) and 2,6-lutidine (0.03 mL) was heated in 2 mL of ethanol at 100 °C for 1 h, which resulted in quantitative deprotection of the chloroacetamide. Treatment with 0.5 mL of aqueous saturated $NaHCO_3$ and 0.1 mL of propionic anhydride gave, after workup (aqueous $NaHCO_3$/CH_2Cl_2) and chromatography (ether, $R_f = 0.25$), (2*S*,6*R*)-2-[4′-[(carboxypropyl)oxy]phenoxy]-6-(propanamidomethyl)tetrahydropyran as a crystalline solid (47 mg, 100%). Treatment with ethanolamine (0.2 mL) and K_2CO_3 (50 mg) in ethanol (2 mL) at 50 °C overnight gave, after evaporation of the reaction mixture and chromatography (CH_2Cl_2/MeOH (10:1), $R_f = 0.28$), pure **11** as a colorless solid. Identical procedures yielded **12**−**14** from the corresponding intermediates.

Data for **11**: colorless solid; mp 120−122 °C; $\alpha_D = -189$ ($c = 0.5$, EtOH); HRMS for $C_{18}H_{26}N_2O_5$ (M + H$^+$) calcd 351.1920, found 351.1923.

Data for **12**: colorless solid; mp 121−123 °C; HRMS for $C_{18}H_{26}N_2O_5$ (M + H$^+$): calcd 351.1920, found 351.1923; ^{1}H NMR (500 MHz, $CDCl_3$) δ 7.76, 7.09 (2m, 2 × 2H), 6.59 (br t, 1H, $J = 5$), 5.70 (br d, 1H, $J = 2$), 5.57 (br t, 1H, $J = 5$), 3.84 (t, 2H, $J = 5$), 3.80 (tm, 1H, $J = 9$), 3.63 (q, 2H, $J = 5$), 3.47 (ddd, 1H, $J = 14$, 7, 3), 3.02 (ddd, 1H, $J = 14$, 8, 5), 2.70 (br s, 1H), 2.07−1.92 (m, 4H), 1.80 (dt, 1H, $J = 13$, 3), 1.75 (m, 1H), 1.40 (qd, 1H, $J = 11$, 4), 0.98 (t, 3H, $J = 8$); ^{13}C-NMR (125 MHz, $CDCl_3$) δ 173.9, 167.9, 159.2, 128.8, 128.7, 127.2, 116.1, 95.1, 69.2, 62.4, 43.5, 42.8, 29.6, 29.2, 27.7, 17.2, 9.7.

Data for **13**: colorless solid; mp 149−150 °C; $\alpha_D = +38$ ($c = 0.64$, EtOH); HRMS for $C_{18}H_{26}N_2O_5$ (M + H$^+$) calcd 351.1920, found 351.1923.

Data for **14**: colorless solid; mp 148−149 °C; HRMS for $C_{18}H_{26}N_2O_5$ (M + H$^+$) calcd 351.1920, found 351.1923; ^{1}H NMR (500 MHz, $CDCl_3$) δ 7.73, 6.98 (2m, 2 × 2H), 6.78 (br t, 1H, $J = 5$), 5.97 (br t, 1H, 1H, $J = 5$), 5.15 (dd, 1H, $J = 9$, 2), 3.82 (t, 2H, $J = 5$), 3.73 (m,

(18) The crystal structure of an antibody−hapten complex has been reported for an antibody catalyzing the chorismate mutase reaction: Haynes, M. R.; Stura, E. A.; Hilvert. D.; Wilson, I. A. *Science* **1994**, *263*, 646. As can be appreciated by the present study, stable antibody−substrate, antibody−inhibitor, or antibody−product complexes with 14D9 might not show these molecules in the unstable, transition state orientation C. Nevertheless, if a crystal structure of 14D9 becomes available, our predictions concerning the available space around the hapten and the position of the general acid will have the opportunity to be tested.

1H), 3.67 (ddd, 1H, J = 14, 7, 3), 3.61 (q, 2H, J = 8), 3.09 (m, 2H), 2.19 (q, 2H, J = 8), 1.97 (m, 2H), 1.66 (m, 2H), 1.29 (m, 2H), 1.14 (t, 3H, J = 8); ^{13}C NMR (125 MHz, $CDCl_3$) δ 174.1, 167.9, 159.5, 128.7, 127.6, 115.7, 99.0, 75.1, 62.3, 43.5, 42.8, 30.4, 29.7, 27.3, 21.1, 9.9.

Preparation of Benzylic Ammonium Salts 19–37. General Procedure. *N*-(Hydroxylethyl)-4-(chloromethyl)benzamide or 4-(chloromethyl)benzoic acid (100–500 mg) was treated with the amine in water until the chloride was consumed. The excess amine was then removed under vacuum and the residue diluted with 50 mL of water and acidified with trifluoroacetic acid (TFA) to pH 2. This solution was loaded on a preparative reversed-phase C-18 column (Waters prepak cartridge 500 g installed on a Water Prep LC 4000 system from Millipore). Gradient elution starting with 100% water + 0.1% TFA, increasing 1% of 50:50 acetonitrile/water per minute at 100 mL/min, gave the pure trifluoroacetate salts as the first major peak (detection by UV 254 nm). Impurities including the corresponding benzyl alcohol and some dialkylation products eluted later. The products (yield 50–300 mg) were obtained as colorless solids from the lyophilization of the pure fractions. The purity of these samples exceeded 98% by analytical HPLC (isocratic elution with 97% H_2O + 0.1% TFA, 3% acetonitrile on an RP C-18 Vydac 218TP54, 0.45 × 22 cm, 1.5 mL/min, detection by UV 254 nm).

***N*-(Hydroxyethyl)-4-(aminomethyl)benzamide, TFA Salt (19). 19** was prepared from 100 mg of chloride and 8 mL of aqueous ammonium hydroxide, 2 h at 20 °C: yield of HPLC purified TFA salt: 65 mg; ^{1}H NMR (500 MHz, D_2O) δ 7.83, 7.56 (2d, 2 × 2H, J = 8.3), 4.26 (s, 2H), 3.78 (t, 2H, J = 5.5), 3.55 (t, 2H, J = 5.5); ^{13}C NMR (125 MHz, D_2O) δ 171.6, 137.4, 135.4, 130.0, 128.9, 61.0, 43.6, 43.0; HRMS for $C_{10}H_{14}N_2O_2$ (M + H^+) calcd 195.1134, found 195.1130.

***N*-(Hydroxyethyl)-4-[(methylamino)methyl]benzamide, TFA Salt (20). 20** was prepared from 100 mg of chloride and 5 mL of 40% aqueous methylamine, 2 h at 20 °C: yield of HPLC purified TFA salt 57 mg; colorless solid, HRMS for $C_{11}H_{17}N_2O_2{}^+C_2F_3O_2{}^-$ (M^+) calcd 209.1290, found 209.1283; ^{1}H NMR (300 MHz, D_2O) δ 7.80, 7.52 (2d, 2 × 2H, J = 8), 4.80 (s, 3H), 4.09 (s, 2H), 3.77, 3.64 (2 d, 2 × 2H, J = 6), 2.58 (s, 3H).

***N*-(Hydroxyethyl)-4-[(dimethylamino)methyl]benzamide, TFA Salt (21). 21** was prepared from 200 mg of chloride and 2 mL of 40% aqueous dimethylamine, 15 h at 20 °C: yield of HPLC purified TFA salt: 230 mg; colorless solid; mp 98–100 °C; HRMS for $C_{12}H_{19}N_2O_2{}^+C_2F_3O_2{}^-$ (M^+) calcd 223.1447, found 223.1450; ^{1}H NMR (300 MHz, D_2O) δ 7.92, 7.56 (2d, 2 × 2H, J = 8), 4.35 (s, 2H), 3.76, 3.52 (2t, 2 × 2H, J = 7), 2.84 (s, 6H).

4-[(Dimethylamino)methyl]benzoic Acid, TFA Salt (22). 22 was prepared from 200 mg of chloride and 2 mL of 40% aqueous dimethylamine at 20 °C for 2 h: yield of HPLC purified TFA salt 290 mg; colorless solid; mp 151–153 °C; HRMS for $C_{10}H_{14}NO_2{}^+C_2F_3O_2{}^-$ (M^+) calcd 180.1025, found 180.1034; ^{1}H NMR (300 MHz, D_2O) δ 8.03, 7.56 (2d, 2 × 2H, J = 8), 4.35 (s, 2H), 2.83 (s, 6H).

Trimethyl[(4-carboxyphenyl)methyl]ammonium Trifluoroacetate (23). 23 was prepared from 200 mg of chloride and 1 mL of 40% aqueous trimethylamine in 10 mL of water at 80 °C for 3 h: yield of HPLC purified TFA salt 240 mg; colorless solid; mp 218–220 °C; HRMS for $C_{11}H_{16}NO_2{}^+C_2F_3O_2{}^-$ (M^+) calcd 194.1181, found 194.1190; ^{1}H NMR (300 MHz, D_2O) δ 8.13, 7.69 (2d, 2 × 2H, J = 8), 4.58 (s, 2H), 3.13 (s, 9H).

Ethyldimethyl[(4-carboxyphenyl)methyl]ammonium Trifluoroacetate (24). 24 was prepared from 300 mg of chloride and 0.5 mL of dimethylethylamine in 0.5 mL of water at 20 °C for 30 min: yield of HPLC purified material 470 mg; colorless solid; mp 202–203 °C; HRMS for $C_{12}H_{18}NO_2{}^+C_2F_3O_2{}^-$ (M^+) calcd 208.1338, found 208.1331; ^{1}H NMR (300 MHz, D_2O) δ 8.12, 7.18 (2d, 2 × 2H, J = 8), 4.55 (s, 2H), 3.42 (q, 2H, J = 7), 3.03 (s, 6H), 1.47 (t, 3H, J = 7).

Diethylmethyl[(4-carboxyphenyl)methyl]ammonium Trifluoroacetate (25). 25 was prepared from 300 mg of chloride and 1 mL of diethylmethylamine in 1 mL of water at 20 °C for 3 h: yield of HPLC purified TFA salt 270 mg; colorless solid; mp 200–202 °C; HRMS for $C_{13}H_{20}NO_2{}^+C_2F_3O_2{}^-$ (M^+) calcd 222.1494, found 222.1500; ^{1}H NMR (300 MHz, D_2O) δ 8.12, 7.68 (2d, 2 × 2H, J = 8), 4.54 (s, 2H), 3.38 (m, 4H), 2.95 (s, 3H), 1.44 (t, 6H, J = 7).

Triethyl[(4-carboxyphenyl)methyl]ammonium Trifluoroacetate (26). 26 was prepared from 200 mg of chloride and 0.5 mL of triethylamine in 10 mL of water at 80 °C for 1 h: yield of HPLC purified TFA salt 230 mg; colorless solid; mp 170–172 °C; HRMS for $C_{14}H_{22}NO_2{}^+C_2F_3O_2{}^-$ (M^+) calcd 236.1651, found 236.1658; ^{1}H NMR (300 MHz, D_2O) δ 8.08, 7.15 (2d, 2 × 2H, J = 8), 4.50 (s, 2H), 3.26 (q, 6H, J = 7), 1.42 (t, 9H, J = 7).

4-[(Ethylmethylamino)methyl]benzoic Acid, TFA Salt (27). 27 was prepared from 200 mg of chloride and 1 mL of methylethylamine in 1 mL of water at 20 °C for 2 h: yield of HPLC purified TFA salt 220 mg; colorless solid; mp 132–134 °C; HRMS for $C_{11}H_{16}NO_2{}^+C_2F_3O_2{}^-$ (M^+) calcd 194.1181, found 194.1189; ^{1}H NMR (300 MHz, D_2O) δ 8.05, 7.57 (2d, 2 × 2H, J = 8), 4.47, 4.26 (2d, 2 × 1H, J = 14), 3.31, 3.24 (2 dq, 2 × 1H, J = 12, 7), 2.26 (s, 3H), 1.32 (t, 3H, J = 7).

4-[(Diethylamino)methyl]benzoic Acid, TFA Salt (28). 28 was prepared from 200 mg of chloride and 1 mL of diethylamine in 1 mL of water at 20 °C for 2 h: yield of HPLC purified TFA salt 235 mg; colorless solid; mp 123–125 °C; HRMS for $C_{12}H_{18}NO_2{}^+C_2F_3O_2{}^-$ (M + H^+) calcd 209.1416, found 209.1428; ^{1}H NMR (300 MHz, D_2O) δ 8.04, 7.57 (2d, 2 × 2H, J = 8), 4.36 (s, 2H), 3.19 (m, 4H), 1.28 (t, 6H, J = 7).

4-[(Propylmethylamino)methyl]benzoic Acid, TFA Salt (29). 29 was prepared from 200 mg of chloride and 1 mL of methylpropylamine in 1 mL of water at 20 °C for 2 h: yield of HPLC purified TFA salt 240 mg; colorless solid; mp 138–140 °C; HRMS for $C_{12}H_{18}NO_2{}^+C_2F_3O_2{}^-$ (M^+) calcd 208.1338, found 208.1345; ^{1}H NMR (300 MHz, D_2O) δ 8.06, 7.57 (2d, 2 × 2H, J = 8), 4.47, 4.27 (2d, 2 × 1H, J = 13), 3.15, 3.02 (2 dt, 2 × 1H, J = 12, 5), 2.77 (s, 3H), 1.75 (m, 2H), 0.92 (t, 3H, J = 7).

4-[(1-Pyrrolidino)methyl]benzoic Acid, TFA Salt (30). 30 was prepared from 1 g of chloride and 3 mL of pyrrolidine in 3 mL of water at 20 °C for 20 h: yield of HPLC purified TFA salt of one fourth of the sample 200 mg; colorless solid; mp 172–174 °C; HRMS for $C_{12}H_{16}NO_2{}^+C_2F_3O_2{}^-$ (M^+) calcd 206.1181, found 206.1188; ^{1}H NMR (300 MHz, D_2O) δ 8.02, 7.55 (2d, 2 × 2H, J = 8), 4.40 (s, 2H), 3.49 (m, 2H), 3.15 (m, 2H), 2.14 (m, 2H), 1.93 (m, 2H).

***N*-Methyl-*N*-[(4-carboxyphenyl)methyl]pyrrolidinium Trifluoroacetate (31). 31** was prepared from one fourth of the crude of **30** and 0.3 mL of iodomethane in 4 mL of methanol/water 1:1 at 37 °C for 20 h: yield of HPLC purified TFA salt 150 mg; colorless solid; mp 205–206 °C; HRMS for $C_{13}H_{18}NO_2{}^+C_2F_3O_2{}^-$ (M^+) calcd 220.1338, found 220.1344; ^{1}H NMR (300 MHz, D_2O) δ 8.08, 7.62 (2d, 2 × 2H, J = 8), 4.56 (s, 2H), 3.61 (m, 2H), 3.43 (m, 2H), 2.95 (s, 3H), 2.22 (m, 4H).

***N*-Ethyl-*N*-[(4-carboxyphenyl)methyl]pyrrolidinium Trifluoroacetate (32). 32** was prepared from one fourth of the vacuum dried crude of **30** and 0.5 mL of iodoethane in 4 mL of methanol/water 1:1 at 37 °C for 3 days: yield of HPLC purified TFA salt 120 mg; colorless solid; mp 140–142 °C; HRMS for $C_{14}H_{20}NO_2{}^+C_2F_3O_2{}^-$ (M^+) calcd 234.1494, found 234.1486; ^{1}H NMR (300 MHz, D_2O) δ 8.05, 7.62 (2d, 2 × 2H, J = 8), 4.50 (s, 2H), 3.54, 3.42 (2m, 2 × 2H), 3.23 (q, 2H, J = 7), 2.15 (m, 4H), 1.42 (t, 3H, J = 7).

***N*-Propyl-*N*-[(4-carboxyphenyl)methyl]pyrrolidinium Trifluoroacetate (33). 33** was prepared from one fourth of the vacuum dried crude of **30** and 0.5 mL of iodopropane in 4 mL of methanol/water 1:1 at 37 °C for 8 days: yield of HPLC purified TFA salt 50 mg; soluble only in DMSO/water mixture; colorless solid; 170–174 °C; HRMS for $C_{15}H_{22}NO_2{}^+C_2F_3O_2{}^-$ (M^+) calcd 248.1651, found 248.1648; ^{1}H NMR (300 MHz, 20% D_2O/80% DMSO-d_6) δ 8.03, 7.65 (2d, 2 × 2H, J = 8), 4.56 (s, 2H), 3.40 (m, 4H), 3.00 (m, 2H), 2.05 (m, 4H), 1.82 (m, 2H), 0.86 (t, 3H, J = 7).

4-[(1-Piperidino)methyl]benzoic Acid, TFA Salt (34). From 300 mg of chloride and 1 mL of piperidine in 1 mL of water at 20 °C for 20 h: yield of HPLC purified TFA salt 234 mg; colorless solid; mp 176–178 °C; HRMS for $C_{13}H_{18}NO_2{}^+C_2F_3O_2{}^-$ (M^+) calcd 220.1338, found 220.1344; ^{1}H NMR (300 MHz, D_2O) δ 8.04, 7.54 (2d, 2 × 2H, J = 8), 4.31 (s, 2H), 3.44 (br d, 2H, J = 11), 2.94 (td, 2H, J = 11, 2), 1.88 (br d, 2H, J = 13), 1.74 (m, 1H), 1.72 (tt, 2H, J = 13, 2), 1.42 (qt, 1H, J = 10, 2).

***N*-Methyl-*N*-[(4-carboxyphenyl)methyl]piperidinium Trifluoroacetate (35). 35** was prepared from 200 mg of chloride and 0.5 mL of *N*-methylpiperidine in 10 mL of water at 80 °C for 1 h: yield of HPLC purified TFA salt 70 mg; colorless solid; mp 206–207 °C;

HRMS for $C_{14}H_{20}NO_2^+C_2F_3O_2^-$ (M^+) calcd 234.1494, found 234.1499; ^1H NMR (300 MHz, D_2O) δ 8.07, 7.63 (2d, 2 × 2H, J = 8), 4.56 (s, 2H), 3.36 (m, 4H), 2.96 (s, 3H), 1.92 (m, 4H), 1.72 (m, 1H), 1.60 (m, 1H).

***N*-Ethyl-*N*-[(4-carboxyphenyl)methyl]piperidinium Trifluoroacetate (36).** **36** was prepared from 200 mg of chloride and 0.5 mL of *N*-ethylpiperidine in 10 mL of water at 80 °C for 5 h: yield of HPLC purified TFA salt 240 mg; colorless solid; mp 108−110 °C; HRMS for $C_{15}H_{22}NO_2^+C_2F_3O_2^-$ (M^+) calcd 248.1651, found 248.1659; ^1H NMR (300 MHz, D_2O) δ 8.10, 7.65 (2d, 2 × 2H, J = 8), 4.53 (s, 2H), 3.35 (m, 6H), 1.93 (m, 4H), 1.75 (m, 1H), 1.58 (m, 1H), 1.45 (t, 3H, J = 7).

***N*-Propyl-*N*-[(4-carboxyphenyl)methyl]piperidinium Trifluoroacetate (37).** **37** was prepared from 400 mg of chloride and 1 mL of piperidine in 1 mL of water at 20 °C for 2 days, followed by removal of excess amine under vacuum and reaction with 0.5 mL of iodopropane in 3 mL of methanol/water (50:50) for 7 d at 37 °C: yield of HPLC purified TFA salt 25 mg; soluble only in DMSO/water mixtures; colorless solid; mp 197−200 °C; HRMS for $C_{16}H_{24}NO_2^+C_2F_3O_2^-$ (M^+) calcd 262.1807, found 262.1815; ^1H NMR (300 MHz, 20% D_2O/80% DMSO-d_6) δ 8.03, 7.59 (2d, 2 × 2H, J = 8), 4.60 (s, 2H), 3.20 (m, 4H), 3.07 (m, 2H), 1.80 (m, 6H), 1.58, 1.43 (2m, 2 × 1H), 0.88 (t, 3H, J = 7).

(*Z*)- and (*E*)-*N*-(Hydroxyethyl)-4-(3′-methoxy-2′-ethyl-2′-propen-1′-yl)benzamides 38 and 39. A solution of 2-ethylacrolein (2.0 g) in 50 mL of dry diethyl ether was added dropwise to a magnetically stirred suspension of lithium aluminum hydride (0.5 g) in 100 mL of dry diethyl ether at 0 °C. After 10 min, the suspension was treated with ethyl acetate (2.5 mL) and 10 g of silica gel for 20 min at 0 °C. The silica gel was filtered off and washed with ether, and the filtrate concentrated by evaporation at 40 °C and atmospheric pressure. Half of this crude 2-ethyl-2-propen-1-ol was mixed with ethyl 4-iodobenzoate (0.5 g), *N*-methylpyrrolidone (2 mL), and solid $NaHCO_3$ (0.3 g). The solution was flushed with argon and heated at 150 °C with 5 mg of $Pd^{II}Cl_2$ for 5 h.[19] Workup (ethyl acetate/water) and chromatography (10:1 hexane/ethyl acetate, R_f 0.3) gave ethyl 4-(3′-oxo-2′-ethylprop-1′-yl)benzoate (335 mg). This aldehyde gave its dimethyl acetal (320 mg) by reaction with 10 mg of camphorsulfonic acid (CSA) in trimethyl orthoformate and methanol (3 mL each) at 37 °C for 3 h, followed by neutralization (3 drops of aqueous NH_3), evaporation, and chromatography (hexane/ethyl acetate (20:1), R_f 0.4). Half of this acetal (160 mg) was treated at 0 °C with hexamethyldisilazane (HMDS, 0.26 mL) and iodotrimethylsilane[20] (0.17 mL) in dry carbon tetrachloride (3 mL). Heating at 60 °C for 5 h, followed by workup (ethyl acetate/aqueous $NaHCO_3$) and chromatography (hexane and then 3% ethyl acetate in hexane, R_f 0.4) gave a pure isomeric mixture of the corresponding (*E*)- and (*Z*)-enol ethers (100 mg), which was treated with ethanolamine at 50 °C overnight to give, after workup (water/dichloromethane), **38** and **39** as a clean 1:1 isomeric mixture (110 mg). These were separated by preparative reversed-phase HPLC (Waters 500 cartridge as above, load as 100 mL solution in 85:15 water/acetonitrile, gradient elution increasing 0.5% acetonitrile/min) and gave first **39** (40 mg of solid after lyophilization) and then **38** (45 mg of solid after lyophilization) as two baseline separated fractions.

Data for **38**: colorless solid; mp 58−60 °C; HRMS for $C_{15}H_{21}NO_3$ ($M + H^+$) calcd 264.1600, found 264.1598; ^1H NMR (300 MHz, $CDCl_3$) δ 7.67, 7.28 (2d, 2 × 2H, J = 8.5), 6.58 (br t, 1H, J = 5), 5.92 (s, 1H), 3.83 (t, 2H, J = 5), 3.63 (q, 2H, J = 5), 3.62 (s, 3H), 3.45 (s, 2H), 1.82 (q, 2H, J = 7.5), 0.93 (t, 3H, J = 7.5), NOE irradiation on δ 1.82 gives 3% on δ 5.92, irradiation on δ 3.45 gives <0.5% on δ 5.92; ^{13}C NMR (125 MHz, $CDCl_3$) δ 168.7, 145.3, 142.5, 131.4, 128.9, 126.9, 118.2, 62.6, 59.4, 42.9, 33.0, 24.2, 12.9.

Data for **39**: colorless solid; mp 78−82 °C; HRMS for $C_{15}H_{21}NO_3$ ($M + H^+$) calcd 264.1600, found 264.1597; ^1H NMR (300 MHz, $CDCl_3$) δ 7.68, 7.24 (2d, 2 × 2H, J = 8.5), 6.70 (br t, 1H, J = 5), 5.81 (s, 1H), 3.82 (t, 2H, J = 5), 3.62 (q, 2H, J = 5), 3.58 (s, 3H), 3.22 (s, 2H), 1.96 (q, 2H, J = 7.5), 0.89 (t, 3H, J = 7.5); NOE irradiation on δ 3.22 give 6% on δ 5.81, irradiation on δ 5.81 give 4% on δ 3.22 and 0% on δ 1.96; ^{13}C NMR (125 MHz, $CDCl_3$) δ 168.7, 144.7, 143.4, 131.8, 129.0, 126.9, 118.7, 62.4, 59.5, 42.8, 37.4, 19.9, 12.4.

(19) Chalk, A. J.; Magennis, S. A. *J. Org. Chem.* **1976**, *41*, 273, 1206.
(20) Miller, R. D.; McKean, D. R. *Tetrahedron Lett.* **1982**, *23*, 323.

B. Antibody Assays. Antibodies. Monoclonal antibodies against **1** and **2**, which were raised in conjunction with a previous project,[4] were obtained from ascites fluid grown from the individual hybridoma cell lines, and purified to homogeneity by ammonium sulfate precipitation followed by anion exchange and protein G chromatography.[21] The antibodies were dialyzed in 50 mM bis-tris([bis(hydroxyethyl)amino]-tris(hydroxymethyl)methane) and 100 mM NaCl at pH 6.0 or 7.0. The concentration of antibody was measured by UV at 280 nm as c (mg/mL) = Abs/1.4. The concentration of antibody active sites was then measured in the catalytic assay by quantitative titration with the hapten as described before (ref 8). The catalytic activity of each antibody is reported per unit of active sites as measured by titration with the hapten.

Stock Solutions. Substrates were used as 25 mM stock solutions in 1:1 1 mM NaOH in water/acetonitrile. These solutions were stable for months at −20 °C. The amine inhibitors were used as 10 mM stock solutions of their purified salts in water.

Semipreparative Experiments. A 0.1 mL sample of stock solution of substrate **4** or **5** was added to 2.5 mL of a solution of a 30 μM antibody solution in 50 mM morpholinoethanesulfonic acid buffer, 90 mM NaCl, and 10 mL of NaCN, pH 5.5. After incubation at 37 °C for 5−7 days (the amount of product formed was measured at that point by HPLC), the solution was diluted with 8 mL of buffer and reconcentrated to 2.5 mL by centrifugation in centriprep-10 concentrator tubes from Amicon (dialysis membrane 10 kDa). This operation was repeated twice, after which the antibody solution was reused for the next experiment. The combined filtrates were saturated with NaCl and extracted with ethyl acetate. The solvent was evaporated and the residue dissolved in 5 mL of water and treated with sodium borohydride (10 mg). The solution was then acidified to pH 3 with HCl and loaded on a semipreparative C-18 reversed-phase column (Vydac 1.0 × 22 cm, 4 mL/min). Gradient elution increasing 0.5% acetonitrile/min gave the pure alcohol **9** as the first fraction, followed by unreacted substrate **4** or **5**. The fractions containing **9** were lyophilized, redissolved in anhydrous acetonitrile, and treated with 10 mg of 4-(dimethylamino)-pyridine and 5 μL of (*S*)-methoxy(trifluoromethyl)phenylacetyl chloride at 20 °C for 2 h, and then diluted with ethyl acetate and washed with 1 N HCL, aq. sat. $NaHCO_3$ and aqueous saturated NaCl. The product was purified by preparative TLC (elution with ethyl acetate, R_f 0.35) and analyzed for stereoisomeric purity by ^1H NMR by integration of the aromatic signal at δ 7.13 (minor, derivative of (*R*)-**9**) and 7.10 (major, derivative of (*S*)-**9**).

Data for **9**: colorless hygroscopic solid; MS (FAB+, m/z) for $C_{13}H_{19}NO_3$ (237) 238 ($M + H^+$), 260 ($M + Na^+$); ^1H NMR (300 MHz, D_2O) δ 7.70, 7.35 (2d, 2 × 2H, J = 8.5), 3.75 (t, 2H, J = 6), 3.51 (t, 2H, J = 6), 3.46 (m, 2H), 2.79 (dd, 1H, J = 13.5, 6), 2.48 (dd, 1H, 13.5, 8.5), 1.96 (m, 1H), 0.85 (d, 3H, J = 7).

Data for **9** bis-(*S*)-Mosher ester (racemate): colorless oil; MS (FAB+, m/z) for $C_{33}H_{33}NF_6O_7$ (669) 670 ($M + H^+$); ^1H NMR (300 MHz, $CDCl_3$) δ 7.53 (m, 6H), 7.42 (m, 3H), 7.37 (m, 3H), 7.13, 7.10 (2d, 2 × 0.5H, J = 8.5), 6.20 (br t, 1H), 4.58, 4.48 (2dt, 2 × 1H, J = 11, 5.5), 4.25, 4.19, 4.11, 4.08 (4 dd, 4 × 0.5H, J = 11, 5.5), 3.80 (q, 2H, J = 5.5), 3.58, 3.57 (2q, 2 × 1.5H, J = 1), 3.56 (q, 3H, J = 1), 2.73, 2.71 (2dd, 2 × 0.5H, J = 14, 6.5), 2.50, 2.48 (2dd, 2 × 0.5H, J = 14, 8), 2.18 (m, 1H), 0.94, 0.92 (2d, 2 × 1.5H, J = 6).

The four antibody samples used in the experiments above were recovered and dialyzed into bis-tris pH 7.0 buffer. A 0.1 mL sample of a 25 mM stock solution of **6** was added, and the concentrated antibody solutions (2.5 mL) and product formation were followed by HPLC (see Table 2). The solutions were then diluted and reconcentrated as above using centriprep tubes, and the filtrates saturated with NaCl and extracted with ethyl acetate. The products were purified by preparative TLC (ethyl acetate/hexane (2:1), R_f(**6**) = 0.6, R_f(**7**) = 0.2), and the ketone was analyzed on a chiralpak AS column (see below). See ref 7 for a large scale procedure with antibody 14D9.

Resolution of 7 and 18. Samples of the racemic ketones were prepared by hydrolysis of enol ethers **6** and **10** in water at pH 2 and purified by chromatography on silica gel.

Data for **7**: colorless crystals; mp 75−77 °C; HRMS ($M + H^+$) calcd 262.1443, found 262.1436; ^1H NMR (500 MHz, $CDCl_3$) δ 7.69,

(21) (a) Köhler, G.; Milstein, C. *Nature* **1975**, *256*, 495. (b) Enguall, E. *Methods Enzymol.* **1980**, *70*, 419.

7.21 (2m, 2 × 2H), 6.78 (br t, 1H), 3.81 (br m, 2H), 3.61 (q, 2H, J = 5), 3.15 (dd, 1H, J = 14, 4), 3.04 (br m, 1H), 2.60 (dd, 1H, J = 14, 9), 2.36 (m, 2H), 2.08 (m, 2H), 1.96 (m, 1H), 1.81 (br s, 1H), 1.74 (m, 1H), 1.53 (ddd, 1H, J = 23, 11, 7); ^{13}C NMR (125 MHz, $CDCl_3$) δ 220.0, 168.4, 144.0, 132.1, 129.1, 127.2, 62.1, 50.7, 42.8, 38.1, 35.3, 29.0, 20.5. Anal. Calcd for $C_{15}H_{19}NO_3$ (261.31): C, 68.94; H, 7.33; N, 5.36. Found: C, 68.96; H, 7.65; N, 5.53.

Data for **18**: colorless crystals; mp 92−94 °C; HRMS for $C_{16}H_{21}NO_3$ ($M + H^+$) calcd 276.1600, found 276.1593; ^{1}H NMR (300 MHz, $CDCl_3$) δ 7.66, 7.20 (2d, 2 × 2H, J = 8.5), 6.74 (br t, 1H, J = 5.5), 3.80 (t, 2H, J = 5.5), 3.58 (q, 2H, J = 5.5), 3.21 (dd, 1H, J = 14, 5), 2.65−2.25 (m, 4H), 2.03 (m, 2H), 1.83 (m, 1H), 1.62 (m, 2H), 1.32 (m, 1H); ^{13}C NMR (125 MHz, $CDCl_3$) δ 212.4, 168.5, 144.5, 131.9, 129.3, 129.2, 127.0, 62.2, 52.2, 42.8, 42.1, 35.4, 33.6, 28.0, 25.0.

Small amounts of **7** and **18** (6 × 0.1 mL of 2 mg/mL solution in 7:3 hexane/2-propanol, 1.2 mg of each) were resolved on a chiralpak AS column (0.45 × 22 cm, 1.0 mL/min of hexane/2-propanol (7:3)): t_R((+)-**7**) = 9.2 min, t_R((−)-**7**) = 12.5 min, t_R((+)-**18**) = 7.7 min, t_R((−)-**18**) = 9.8 min. Each isolated sample was 98% pure when reanalyzed on the chiral column. The solvent was removed, and the vacuum-dried samples were redissolved in 0.5 mL of water/acetonitrile (50:50). These stock solutions (approximately 10 mM) were used for competitive inhibition assays. The concentrations were corrected by integration of the peak corresponding to the ketones in the kinetic assay (see below).

Kinetic Measurements. Michaelis−Menten Kinetics. For each substrate and antibody, assays were set up by dilution of a stock solution of substrate plus internal standard with either 0.1−1.5 mg/mL antibody in buffer or buffer alone, using 5−6 different substrate concentrations (50 (2×), 65 (2×), 100, 200, 350, 500, 700 μM). Product formation in each assay below 5% conversion was followed by reversed-phase HPLC. See ref 8 for the detailed procedure and HPLC conditions. The uncatalyzed reaction rate was calculated as an average from the rates measured in the different "buffer only" assays and then subtracted from each antibody assay. The kinetic constants K_m and V_{max} were derived from the x- and y-intercepts in the linear double reciprocal plot of this net rate as $1/V$ vs substrate concentration as $1/S$. The lines were constructed from 5−8 points and gave correlation coefficients of $0.930 < r^2 < 1.000$. The catalytic constant k_{cat} was obtained by dividing V_{max} by the binding site concentration as measured by quantitative titration of the activity of each antibody preparation with the hapten at 100 μM substrate **4** (ref 8).

Competitive Inhibition. A 10 μL sample of prediluted inhibitor solution in buffer was added to 115 μL of a premixed solution of antibody (0.5−1.5 mg/mL), substrate **4**, and internal standard (*N*-ethylbenzamide) in bis-tris (50 mM, pH 6.0) and 100 mM NaCl. A solution containing no inhibitor and a solution containing 250 μM hapten were also used to estimate the catalyzed and the uncatalyzed reaction rates. Two sets of four inhibitor concentrations (5, 10, 20, and 40 μM when K_i < 20 μM, 25, 50, 100, and 200 μM when K_i < 100 μM, and 100, 200, 400, and 800 μM when K_i < 400 μM) were prepared with [**4**] = 100 and 300 μM (final concentrations). The reaction rates at 37 °C below 5% conversion were measured by HPLC in each assay (Asahipac ODP-50 C-18, 0.45 × 22 cm, 0.8 mL/min isocratic elution, 77% water + 0.1% TFA, 23% acetonitrile, t_R(product) = 6.2 min, t_R(standard) = 10.5 min, t_R(**4**) = 24 min, detection by UV 240 nm). After correction for the uncatalyzed rate, obtained from the assay with excess hapten inhibitor, the observed rates were plotted as $1/V$ vs the inhibitor concentration [i] (Dixon plot).[16] The lines obtained at [S] = 100 μM and [S] = 300 μM (four points, $0.98 < r^2 < 1.00$) intersect with the horizontal line reported at $1/V = 1/V_{max}$. The competitive inhibition constant K_i for each inhibitor was obtained as the average of the negative coordinates of these two intersection points on the horizontal [i] axis. The two values differed by 0−20%, so that an error margin of ±20% should be taken on these constants.

Acknowledgment. We thank Prof. R. A. Lerner, Prof. K. N. Houk, Prof. E. Keinan, and Prof. D. Hilvert for helpful suggestions and critical reading of the paper. We gratefully acknowledge the National Institutes of Health (Grant GM 49736 to J.-L.R.) for financial support.

Supplementary Material Available: Text, figures, and tables giving the data for the crystal structure of **15** and the method of data collection (6 pages); tables listing the observed and calculated structure factors for **15** (4 pages). This material is contained in many libraries on microfiche, immediately follows this article in the microfilm version of the journal, and can be ordered from the ACS; see any current masthead page for ordering information.